*Title Page - include author details here only!

Cross gender-age trabecular texture analysis in cone beam computed tomography

Haibin Ling, PhD[1], Xiong Yang, MSS[2], Peiyi Li, PhDS[3], Vasileios Megalooikonomou, PhD[4], Yong Xu, PhD[5], Jie Yang, DDS, MMS, MS, DMD[6]

1-Assistant Professor. Department of Computer and Information Sciences, Temple University, Philadelphia, Philadelphia, USA

2-Visiting MS student, Department of Computer and Information Sciences, Temple University, Philadelphia, Philadelphia, USA

3-PhD student, Department of Computer and Information Sciences, Temple University, Philadelphia, Philadelphia, USA

4-Professor, Department of Computer and Information Sciences, Temple University, Philadelphia, Philadelphia, USA

5-Professor, School of Computer Science and Engineering, South China University of Technology, Guangzhou, China

6-Professor and Director. Division of Oral and Maxillofacial Radiology, Temple University School of Dentistry, and Professor, Department of Diagnostic Imaging, Temple University School of Medicine, Philadelphia, USA

Address of correspondence : Haibin Ling, Department of Computer and Information Sciences, Temple University, Philadelphia, Philadelphia, 19122 USA; E-mail: hbling@temple.edu

Cross gender-age trabecular texture analysis in cone beam computed tomography

Purposes: To investigate whether multiple texture features in different regions-of-interest (ROIs) on cone beam computed tomography (CBCT) are correlated with gender-age variation of trabecular patterns.

Methods: CBCT volumes from 96 subjects were used. The data set was divided into four gender-age subgroups including male younger (MY) than 40 years, male older (MO) than 40 years, female younger (FY) than 40 years, and female older (FO) than 40 years. For each volume, cubes containing trabecular patterns at four ROIs in the jaws were manually cropped. Eighteen distinct texture features were calculated and their correlation with gender-age variations at different ROIs was studied through t-test statistical analysis.

Results: For the 432 test pairs with different gender-age groups at different ROIs and texture features tested, 149 of them were shown to be statistically different at the 0.05 level and 60 at the 0.001 level. These features can therefore capture changes in trabecular patterns and have the potential to be used for trabecular analysis. Furthermore, fractal features were found to be better than intensity features in separating different gender-age groups. Trabecular patterns in the body of the mandible were more correlated with gender-age changes than other ROIs.

Conclusions: Multiple texture features on CBCT were found to be correlated with the cross gender-age variation of trabecular patterns. The results support the use of CBCT for advanced trabecular analysis, including osteoporosis screening tools in the jaws.

Keywords: cone-beam computed tomography, osteoporosis, radiology, fractals, computer -assisted image analysis

Introduction

As a major health problem in the United States, osteoporosis afflicts 55% of Americans aged 50 and above.[1] Early diagnosis of osteoporosis is very important to prevent more serious complications such as hip fracture. The current gold standard for osteoporosis diagnosis for senior patients is based on the bone mineral density (BMD) measured by the dual energy X-ray absorptiometry (DEXA) in the hip and spine region.[2] However, when applied to routine examination for osteoporosis screening, such a gold standard may introduce a significant financial burden.

A potential low cost osteoporosis prescreening method is through the analysis of dental imaging data, which is collected during routine clinical dental examination at almost no additional cost. In particular, trabecular bone structures in the jaws have been studied for their correlation with bone porosity.[3-7] Despite these studies, it remains an open problem to effectively use dental data for osteoporosis prescreening. One of the major reasons lies in the insufficiency to use a limited number of features. In particular, most previous work studies only a few image features (mostly one, often restricted to one region-of-interest), which are not discriminative enough for osteoporosis prescreening due to the large variance and noise in dental data. In fact, many researchers have pointed out the necessity of introducing advanced algorithms to integrate richer image features for dental image-based osteoporosis prescreening.[5,6,8]

The objective in this study was to investigate multiple texture features and multiple regions-of-interest (ROI) in cone beam computed tomography (CBCT) that are correlated with the change in trabecular patterns. Based on the fact that trabecular patterns vary across gender and age,[9] it was hypothesized that these features and ROIs provide discriminative information for cross gender-age trabecular analysis in the jaws. Consequently, CBCT volumes from different gender-age groups were used to explore the discriminative power of different texture features.

Materials and Methods

CBCT Data Capture

In order to evaluate the proposed method, a dataset was used which contains 96 anonymized 3D CBCT volumes from four gender-age subgroups including female younger (FY) than 40 years, female older (FO) than 40 years, male younger (MY) than 40 years, and male older (MO) than 40 years. In general, senior patients have a high probability to be osteoporotic or to have osteopenia when compared with young patients. In the clinic it was also found that some female patients showed osteoporotic changes in their 40s. Therefore 40 years of age was used as a cut off in our experiment. Table 1 gives a summary of the gender-age distribution of the subjects. The dataset was obtained from 96 dental implant patients who had no pathology in the jaws. The CBCT scan was obtained by using an i-Cat machine (Imaging Science International, Inc., Hatfield, PA, USA) with 0.3 mm voxel sizes, 14 bits grayscales, and 8.9 second scan times. The number of slices in one CBCT volume is 327. The project was approved by our institutional review board (IRB).

No particular calculation was performed to determine the total number of samples and all 96 volumes in the original collection were used. The differences between the sample sizes of the groups were taken into account when performing statistical analysis. In particular, the sample sizes were used in the t-tests.

For each volume, a dentist manually cropped eight cubes from eight different locations in the jaws, including areas apical to the maxillary left and right premolars, mandibular left and right lateral incisors and first molars, and left and right condyles. Each cube is a volume of 19×19×19 voxels containing trabecular structures of size 5.7×5.7×5.7 mm^3. The size was chosen to maximally

enclose a trabecular pattern while containing little non-trabecular material. Some example cubes in the dataset are shown in Figure 1. In the rest of the paper such cubes were called trabecular cubes. Considering the left-right symmetry, the eight locations were grouped into four ROIs including ROI 1 (the maxillary premolars), ROI 2 (the mandibular first molars), ROI 3 (the mandibular lateral incisors), and ROI 4 (the left and right condyles). The left-right symmetry was not calculated and the group of left-right ROIs increased the samples in the statistical analysis.

TEXTURE FEATURES

First, the set of collected trabecular cubes was defined as $P = \{p_1, p_2, ..., p_N\}$, where $N = 768 = 96 \times 8$ is the number of trabecular cubes cropped from the 96 dental CBCT volumes. Each cube $p \in P$ has $19 \times 19 \times 19$ voxels and $p(i, j, k)$ indicates the CBCT intensity of the (i, j, k)-th voxel in p, $1 \le i, j, k \le 19$. In this paper the following texture features were explored:

1. *Mean intensity* $\mu(p)$. The mean intensity of a cube p was defined as

$$\mu(p) = \frac{1}{M} \sum_{i=1}^{19} \sum_{j=1}^{19} \sum_{k=1}^{19} p(i, j, k),$$

where $M = 6859 = 19 \times 19 \times 19$ is the number of voxels in a cube.

2. *Intensity histogram* $h(p) = (h_1(p), h_2(p), ..., h_8(p))$. The intensity histogram captures the intensity distribution within a trabecular cube p and therefore provides much richer information than the simple mean intensity. Due to its strong descriptive power, intensity histogram has been recently popularly used in image processing and pattern recognition for image and texture description.[10,11] In this study, eight intensity bins were defined as $(\tau_m, \tau_{m+1}] : m = 1, ..., 8$, such that τ_1 and τ_9 indicate respectively the lower and upper bounds of intensities in the cube p as below

$$\tau_1 = \min_{1\le i,j,k\le 19} p(i,j,k) - 1,$$
$$\tau_9 = \max_{1\le i,j,k\le 19} p(i,j,k).$$

$\tau_{m+1} = \tau_m + (\tau_9 - \tau_1)/8$ for $m = 1,...,7$. Then, the m-th component of the intensity histogram of the cube p was defined as

$$h_m(p) = \#(\{(i,j,k) : \tau_m < p(i,j,k) \le \tau_{m+1}\}),$$

where '#' indicates the cardinality of a set. More specifically, $h_m(p)$ was the number of voxels whose intensities fell in the range $(\tau_m, \tau_{m+1}]$. Eight bins were used mainly for two reasons. First, by using eight bins, each bin received an average of about 857 (≈6859/8) voxels, which were sufficiently large for constructing statistically meaningful histograms. Second, very large numbers of bins were not used since they might be sensitive to intensity noises and histogram quantization problems, which have been observed in the field of pattern recognition and image analysis.[12]

3. *Fractal dimension* $\psi(p)$. Fractal dimension (FD) has been used to capture trabecular texture information.[4,13-15] For a trabecular cube p, a 3D point set was first created as $\Lambda = \{(i,j,k) : p(i,j,k) > \tau\}$, where $\tau = \tau_1 + 0.24 \times (\tau_9 - \tau_1)$ was the threshold to filter out irrelevant background voxels in p. The constant number 0.24 was determined according to the visual inspection. More specifically, the threshold helped to discard the majority of background voxels, and therefore allowed the fractal dimension to focus on trabecular voxels. In other words, when using this threshold, the point set Λ contained most of the trabecular vodels and ignores the majority of background voxels. Then $\psi(p)$ was calculated as the fractal dimension of set Λ using the box-counting approach.[16] Specifically, let the three-dimensional Euclidean space be covered by a mesh of three-dimensional cubes with side length r (i.e., r-mesh) and a counting function

$c(\Lambda, r)$ was defined as the number of r-mesh hypercubes that intersect Λ. Then the box-counting fractal dimension $\psi(p)$ was defined as

$$\psi(p) = \lim_{r \to 0} \frac{\log c(\Lambda, r)}{-\log r},$$

In practice, to approximate the process of $r \to 0$, the slope of $\log(c(\Lambda, r))$ was estimated for a decreasing side-length sequence, $r = 16,8,4,2$ (such that $\log r = 4,3,2,1$), using the least squares method.

4. *Multifractal spectrum* $\varphi(p) = (\varphi_1(p), \varphi_2(p), ..., \varphi_8(p))$. Due to the complexity of trabecular patterns, it may be insufficient to describe them using a single fractal dimension. Multiple-fractal spectrum (MFS) is a natural extension to overcome this limitation.[17,19] A cube p was first partitioned into eight disjoint point sets $\{\Lambda_1, \Lambda_2, ..., \Lambda_8\}$ such that

$$\Lambda_m = \{(i, j, k) : \tau_m < p(i, j, k) \le \tau_{m+1}\}, m = 1,2,...,8.$$

Then, the m-th element $\varphi_m(p)$ was defined as the fractal dimension of Λ_m calculated by the box-counting method described above. Eight disjoint sets were used for the same reasons eight bins were used for intensity histogram. The partition procedure provides MFS with robustness against common pattern deformations such as rotation and scaling, since MFS was known to be invariant under the bi-Lipschitz transformation,[17] which subsumes rotation and scaling.

STATISTICAL METHODS

Statistical analysis on the calculated features is needed to study their effect on separating gender-age groups. One approach is to study the variances and covariances of these features among all four gender-age groups through ANOVA. More specifically, for a given feature, the null hypothesis is that the feature generates the same sample mean for all four groups. However, since

a long term purpose of the study is to prepare guidance for feature selection in future statistical prediction tools, more interests have been shown in finding features that can separate two gender-age groups. Consequently, two-sample t-test is more suitable, which is in fact a special case of ANOVA in that only two groups of samples are involved.[18]

The two-sample t-test was used to study the effects of gender-age on the calculated features. Since there were four gender-age groups in the study, six group pairs were created for comparison: (FO, FY), (FO, MO), (FO, MY), (FY, MO), (FY, MY) and (MO, MY). For each gender-age pair, a statistical analysis for each texture feature (out of 18) on each ROI (out of 4) was conducted. As a result, there were in total 432=6×4×18 gender-age test pairs on different ROIs and features, as summarized in Table 2.

For each of the 432 test pairs described above, the two-sample t-test was performed to compare them with null hypothesis (H_0) and alternative hypothesis (H_A) stated below:

H_0: Data of the two categories are from normal distributions with equal means.

H_A: Data of the two categories are from normal distributions with different means.

The test statistic t was defined as

$$t = \frac{(\mu_1 - \mu_2)}{\sqrt{S^2(1/n_1 + 1/n_2)}},$$

where μ_1 and μ_2 are the sample means of the two categories under comparison; n_1 and n_2 are the numbers of samples in the two categories; and S^2 was defined as

$$S^2 = \frac{(n_1 - 1)S_1^2 + (n_2 - 1)S_2^2}{n_1 + n_2 - 2},$$

where S_1^2 and S_2^2 are the sample variances of the two categories respectively. Finally, the *p*-value of the t-test was calculated from the test statistic with respect to the degree of freedom $d = n_1 + n_2 - 2$.

Results

The p-values of the *t*-tests on all gender-age pairs at different ROIs with different features were reported in Table 2. The results with p≤0.05 were highlighted in the table. In addition, all these p-values were plotted in Figure 2 for better illustration. From these results it could be observed that many of the tested features (149 out of 432) were correlated significantly with the gender-age variation at the 0.05 level, with some of them (60 out of 432) at the 0.001 level.

The effectiveness of different features, ROIs, and gender-age pairs in capturing the cross gender-age trabecular variations was also studied in this paper. First, for the effectiveness of a specific feature, the times it correlated significantly (p=0.05) with different gender-age groups at different ROIs have been counted. These numbers were summarized in Table 3. The average effectiveness of the two groups of features, i.e., intensity features and fractal dimension features was also calculated. Second, the numbers of effective features for each gender-age pairs and ROIs were summarized in Table 4. The results illustrated how the proposed features in general were correlated with the variation of trabecular patterns across different gender-age groups at different ROIs.

Discussion

Variations in trabecular bone patterns have been known to reflect bone density change, which suggests the potential of analyzing trabecular patterns for prescreening bone diseases such as osteoporosis. In the past few decades, trabecular bone structure analysis has been studied in various biomedical contexts. The importance of trabecular perforations in the development of osteoporosis has been introduced by Parfitt et al.[20] Previous research has also explained the relation between the profound disintegration of the trabecular bone network and certain bone disease.[21,22] Moreover, studies have shown that the change of the iliac trabecular bone texture can predict osteoporosis in the aspects of its surface texture, volume and thickness.[22]

This study was highly motivated by a series of work towards a potential low cost osteoporosis prescreening method using dental imaging data.[3-7] The widely used dental panoramic radiography is cost-effective since it is often a by-product of routine dental examination. In particular, trabecular bone structures in the jaws have been studied for their correlation to bone porosity. White and Rudolph showed that the trabecular patterns of osteoporosis patients are altered compared to normal subjects.[6] White used fractal dimension to analyze the trabecular bone structure in relation to osteoporosis.[5] Southard et al. showed that the radiographic fractal dimension of the alveolar process bone is correlated with the bone density, using radiographic images.[4] Pham et al. found that panoramic radiographs can be used for assessment of trabecular bone pattern with the aid of a visual index.[3] Yang et al. found that oestrogen deficiency can result in microarchitectural alterations of trabecular bone in both the mandible and the tibia.[7]

Recently, there has been a trend to include cone beam computed tomography in three-dimensional dental examinations.[23] Consequently, it is of interest to study how the trabecular patterns in CBCT correlate with bone porosity. Though the correlation between dental trabecular pattern and osteoporosis has been discovered using dental panoramic radiography and CT,[8,24]

such correlation is not directly available in dental CBCT. One reason lies in that dental CBCT usually has a low resolution (e.g., 0.3~0.4mm), which causes serious blur in trabecular structures which are typically around 0.1 mm in bone thickness. Furthermore, due to the distortion of CBCT measurement from dental CT values, there has been a debate on whether CBCT measurement can be used to infer bone mineral densities.[21,25-27]

Despite the large number of studies showing the positive correlation of texture features with changes in trabecular patterns, there is still a gap towards a practical solution using trabecular analysis for osteoporosis prescreening. Advanced image analysis and statistical learning tools have been expected to be used to address this issue.[5] On the other hand, there have been great progresses in the field of texture analysis and machine learning, as well as their applications to medical image analysis tasks.

In previous studies,[4,6,13-15] only basic texture descriptors, such as intensity and Fourier analysis, have been used to confirm the correlation between the loss of bone mass and the trabecular patterns. It has also been observed that these features by themselves are insufficient to be used for clinical diagnosis or prescreening purposes. A potential way to address this issue is to exploit multiple texture descriptors and combine them together with advanced statistical learning tools. The focus of this paper is on the first step to investigate various high dimensional texture features, including both classical texture descriptors and recently proposed ones.

The result of the study moved one step further along this direction. It demonstrated a series of texture features at four different ROIs for capturing variations in trabecular patterns in dental CBCT. This observation validated the hypothesis that CBCT volumes can be used for cross gender-age analysis of trabecular patterns in the jaws. The results also showed that (1) fractal-analysis based features work generally better than intensity features, (2) FO vs FY and FY vs MO have significantly more effective features than other pairs, which can be attributed to the loss of

bone mass in female seniors, (3) trabecular patterns in the body of the mandible are more correlated with gender-age changes than the maxilla and the mandibular condyles, and (4) the mean intensity is less effective than several fractal dimension features and several components in intensity histogram, which may be due to the fact of instability of CBCT intensity.[21,27]

The results also supported the use of CBCT for the analysis of bone mineral density. Though the detailed trabecular structure is unavailable due to the low resolution used in clinical data, the texture pattern in CBCT still carries useful information reflecting statistics of trabecular patterns, such as the density and regularity of the bone structures. Furthermore, though the CBCT measurement may be distorted from the CT values, some structure-relevant features (e.g., those based on fractal analysis) can still provide discriminative information for separating different trabecular patterns.

In summary, the experiment results validated that the cross gender-age variation of trabecular patterns correlates significantly with many texture features on CBCT. It is highly desirable that the imaging tests used in dentistry are fully exploited to generate the maximum diagnostic information related to systemic conditions such as osteoporosis. The results also showed that rich texture descriptors such as intensity histograms and multifractal spectrum can provide complementary or more discriminative information than previously proposed simple texture descriptors.

In the future, it is expected to combine these features together, using modern machine learning tools such as ensemble learning[28] or kernel learning,[29] to predict the loss of bone mass. Such a predictor will in turn provide the basis of dental image-based osteoporosis prescreening.

REFERENCES

1. National Osteoporosis Foundation. America's Bone Health: The state of osteoporosis and low bone mass in our nation. Washington, DC: National Osteoporosis Foundation, 2002.

2. Kanis JA, Glüer CC. An update on the diagnosis and assessment of osteoporosis with densitometry. Committee of Scientific Advisors, International Osteoporosis Foundation. Osteoporos Int 2000; 11:192-202.

3. Pham D, Jonasson G, Kiliaridis S. Assessment of trabecular pattern on periapical and panoramic radiographs: A pilot study. Acta Odontol Scand 2010; 68:91-97.

4. Southard TE, Southard KA, Lee A. Alveolar process fractal dimension and postcranial bone density. Oral Surg Oral Med Oral Pathol Oral Radiol Endod 2001; 91:486-491.

5. White SC. Oral radiographic predictors of osteoporosis. Dentomaxillofac Radiol 2002; 31:84-92.

6. White SC, Rudolph DJ. Alterations of the trabecular pattern of the jaws in patients with osteoporosis. Oral Surg Oral Med Oral Pathol Oral Radiol Endod 1999; 88:628-635.

7. Yang J, Pham SM, Crabbe DL. High-resolution micro-CT evaluation of mid- to long-term effects of estrogen deficiency on rat trabecular bone. Acad Radiol 2003; 10:1153-1158.

8. Devlin H, Horner K. Diagnosis of osteoporosis in oral health care. J Oral Rehabil 2008; 35:152-157.

9. Parfitt AM. Age-related structural changes in trabecular and cortical bone: cellular mechanisms and biomechanical consequences. Calcif Tissue Int 1984; 36 Suppl 1:S123-128.

10. Jager F, Hornegger J. Nonrigid registration of joint histograms for intensity standardization in magnetic resonance imaging. IEEE Trans Med Imaging 2009; 28:137-150.

11. Han JH, Yang S, Lee BU. A novel 3-D color histogram equalization method with uniform 1-D gray scale histogram. IEEE Trans Image Process 2011; 20:506-512.

12. Rubner Y, Puzicha J, Tomasi C, Buhmann JM. Empirical evaluation of dissimilarity measures for color and texture. Comput Vis Image Und 2001; 84:25-43.

13. Law AN, Bollen AM, Chen SK. Detecting osteoporosis using dental radiographs: a comparison of four methods. J Am Dent Assoc 1996; 127:1734-1742.

14. Ruttimann UE, Webber RL, Hazelrig JB. Fractal dimension from radiographs of peridental alveolar bone. A possible diagnostic indicator of osteoporosis. Oral Surg Oral Med Oral Pathol 1992; 74:98-110.

15. Yi WJ, Heo MS, Lee SS, Choi SC, Huh KH, Lee SP. Direct measurement of trabecular bone anisotropy using directional fractal dimension and principal axes of inertia. Oral Surg Oral Med Oral Pathol Oral Radiol Endod 2007; 104:110-116.

16. Falconer K. Techniques in fractal geometry. Chichester: John Wiley & Sons, 1997.

17. Xu Y, Ji H, Fermuller C. Viewpoint invariant texture description using fractal analysis. Int J Comput Vis 2009; 83:85-100.

18. Keller G. Statistics for management and economics. Mason: Thomson South-Western, 2008.

19. Ji H, Yang X, Ling H, Xu Y. Wavelet domain multifractal analysis for static and dynamic texture classification. IEEE Trans Image Process 2013; 22:286-299.

20. Parfitt AM, Mathews CH, Villanueva AR, Kleerekoper M, Frame B, Rao DS. Relationships between surface, volume, and thickness of iliac trabecular bone in aging and in osteoporosis. Implications for the microanatomic and cellular mechanisms of bone loss. J Clin Invest 1983; 72:1396-1409.

21. Nomura Y, Watanabe H, Honda E, Kurabayashi T. Reliability of voxel values from cone-beam computed tomography for dental use in evaluating bone mineral density. Clin Oral Implants Res 2010; 21:558-562.

22. Eriksen EF. Normal and pathological remodeling of human trabecular bone: three dimensional reconstruction of the remodeling sequence in normals and in metabolic bone disease. Endocr Rev 1986; 7:379-408.

23. Alamri HM, Sadrameli M, Alshalhoob MA, Sadrameli M, Alshehri MA. Applications of CBCT in dental practice: a review of the literature. Gen Dent 2012; 60:390-400.

24. Ardakani FE, Mirmohamadi SJ. Osteoporosis and oral bone resorption: a review. J Maxillofac Oral Surg 2009; 8:121-126.

25. Hua Y, Nackaerts O, Duyck J, Maes F, Jacobs R. Bone quality assessment based on cone beam computed tomography imaging. Clin Oral Implants Res 2009; 20:767-771.

26. Katsumata A, Hirukawa A, Noujeim M, Okumura S, Naitoh M, Fujishita M, et al. Image artifact in dental cone-beam CT. Oral Surg Oral Med Oral Pathol Oral Radiol Endod 2006;101:652-657.

27. Lee S, Gantes B, Riggs M, Crigger M. Bone density assessments of dental implant sites: 3. Bone quality evaluation during osteotomy and implant placement. Int J Oral Maxillofac Implants 2007; 22:208-212.

28. Breiman L. Random forests. Mach Learn 2001; 45:5–32.

29. Vapnik V. The nature of statistical learning theory. New York: Springer-Verlag, 1995

Table 1. Trabecular bone 3D image sample quantity

Group	Male younger than 40 (MY)	Male older than 40 (MO)	Female younger than 40 (FY)	Female older than 40 (FO)
Number of volumes	8	27	13	48

Table 2. P-values of all gender-age pairs over different ROIs and features. The abbreviations used are: MY for Male Younger than 40, MO for Male Older than 40, FY for Female Younger than 40, and FO for Female Older than 40. The four ROIs are: ROI 1 for maxillary premolar, ROI 2 for mandibular first premolar, ROI 3 for mandibular lateral incisor, and ROI 4 for mandibular condyle.

		Intensity Features									Fractal Dimension Features								
		μ	h_1	h_2	h_3	h_4	h_5	h_6	h_7	h_8	ψ	φ_1	φ_2	φ_3	φ_4	φ_5	φ_6	φ_7	φ_8
FO vs FY	ROI 1	0.065	**0.011**	0.240	0.704	**0.050**	**0.028**	0.090	0.234	0.524	0.105	**0.012**	**0.047**	0.926	0.097	**<.001**	**<.001**	0.065	0.279
	ROI 2	**<.001**	**<.001**	0.104	**<.001**	**<.001**	0.576	**<.001**	**<.001**	**<.001**	**<.001**	0.059	**<.001**	**<.001**	**<.001**	**<.001**	**<.001**	**0.023**	**<.001**
	ROI 3	**<.001**	**0.011**	**0.012**	0.480	0.323	0.744	0.202	0.599	**0.039**	**<.001**	**<.001**	0.249	**<.001**	**<.001**	**<.001**	**<.001**	**0.003**	**<.001**
	ROI 4	0.097	**0.002**	**0.001**	0.070	**0.007**	0.676	**0.001**	**0.016**	0.053	0.163	0.260	0.369	0.133	0.215	0.119	0.054	0.182	0.609
FO vs MO	ROI 1	0.710	**0.001**	0.069	**0.033**	0.175	0.600	0.208	0.439	0.829	0.350	0.740	0.078	0.060	0.958	0.160	0.059	0.248	0.285
	ROI 2	0.261	**0.004**	0.603	0.058	0.340	0.583	0.552	0.342	0.610	**0.010**	0.770	0.206	0.127	0.132	0.262	0.887	0.754	0.107
	ROI 3	0.092	**0.015**	0.824	**0.010**	0.183	0.493	**0.006**	0.193	0.667	**0.046**	0.096	**0.041**	0.118	0.926	0.466	**0.040**	0.260	**0.043**
	ROI 4	**0.002**	0.654	0.205	0.103	0.244	0.375	0.134	0.100	0.388	0.354	**<.001**	**0.017**	0.986	0.629	**0.013**	**0.008**	**0.036**	0.413
FO vs MY	ROI 1	0.238	**0.002**	0.108	**<.001**	**0.004**	0.092	0.477	0.804	0.516	0.467	0.854	**0.003**	**0.026**	0.773	0.206	0.396	0.714	**0.044**
	ROI 2	0.235	0.136	0.507	0.390	0.258	0.564	**0.031**	**0.025**	**0.024**	**0.018**	0.735	0.220	0.412	0.380	0.335	**0.048**	**0.017**	**0.021**
	ROI 3	0.736	0.358	0.621	**<.001**	**0.007**	0.962	0.881	0.947	0.998	0.514	0.075	**0.015**	0.339	0.169	**<.001**	**<.001**	0.070	**<.001**
	ROI 4	0.421	0.878	0.238	0.231	0.092	0.054	0.550	0.202	0.309	0.866	0.539	0.056	0.461	0.102	0.145	0.152	0.221	0.503

FY vs MO	ROI 1	**0.040**	0.71	0.824	0.156	0.718	**0.014**	**0.010**	0.097	0.431	**0.024**	**0.031**	0.555	0.205	0.139	**0.015**	**0.009**	0.344	0.918
	ROI 2	**<.001**	**<.001**	0.058	**<.001**	**<.001**	0.262	**<.001**	**<.001**	**<.001**	**<.001**	**0.045**	**<.001**	**<.001**	**<.001**	**<.001**	**<.001**	0.076	**<.001**
	ROI 3	**<.001**	**<.001**	**0.018**	**0.007**	**0.050**	0.896	0.410	0.149	**0.030**	**<.001**	**<.001**	**0.013**	**<.001**	**<.001**	**0.002**	**0.020**	0.290	**0.001**
	ROI 4	**0.007**	**0.035**	**<.001**	0.874	0.329	0.781	**0.046**	0.112	0.250	0.932	**0.003**	0.312	0.174	0.142	**0.002**	**<.001**	**0.008**	0.228
FY vs MY	ROI 1	**0.012**	0.501	0.622	**0.003**	0.258	0.621	0.127	0.270	0.332	**0.047**	0.084	0.270	0.083	0.361	0.198	0.063	0.277	0.292
	ROI 2	0.131	0.108	0.396	0.064	**0.019**	0.329	0.758	0.057	**0.043**	0.128	0.088	**0.040**	0.095	0.079	0.071	0.138	0.655	0.539
	ROI 3	**0.001**	**0.006**	0.109	**<.001**	**0.002**	0.756	0.382	0.602	0.088	**0.040**	0.216	**0.005**	**0.002**	**0.028**	0.163	0.201	0.404	0.109
	ROI 4	0.058	0.053	**0.006**	0.753	**0.001**	0.191	0.060	0.324	0.684	0.221	0.215	0.302	0.087	**0.029**	**0.025**	**0.026**	0.053	0.321
MO vs MY	ROI 1	0.404	0.725	0.732	**0.028**	0.171	**0.046**	0.940	0.714	0.595	0.982	0.967	0.072	0.456	0.812	0.737	0.720	0.700	0.230
	ROI 2	0.080	**0.005**	0.317	0.091	0.105	0.825	**0.013**	**0.007**	**0.014**	**<.001**	0.902	0.052	0.105	0.080	0.100	**0.042**	0.052	0.151
	ROI 3	0.261	0.283	0.528	0.351	0.146	0.597	0.079	0.286	0.778	0.081	**0.006**	0.467	0.867	0.199	**0.039**	0.176	0.713	0.074
	ROI 4	0.463	0.690	0.637	0.670	**0.034**	0.240	0.686	0.700	0.643	0.367	0.351	0.839	0.520	0.178	0.410	0.205	0.336	0.995

Table 3. The effectiveness of different features. NoT is short for Number of Tests, which is the number of the tests in which a feature significantly ($p \leq 0.05$) distinguishes two categories. For example, in the first column of the first row, NoT=9 means that, in the first column of Table 2, 9 out of the 24 p-values corresponding to μ are smaller than or equal to 0.05. PoT is short for Percentage of Tests, which was defined as PoT= NoT/24.

	Intensity Features									Fractal Dimension Features								
Feature	μ	h_1	h_2	h_3	h_4	h_5	h_6	h_7	h_8	ψ	φ_1	φ_2	φ_3	φ_4	φ_5	φ_6	φ_7	φ_8
NoT	9	13	5	10	11	3	8	5	7	11	8	10	6	6	11	13	5	8
PoT	37.5	54.2	20.8	41.7	45.8	12.5	33.3	20.8	29.2	45.8	33.3	41.7	25.0	25.0	45.8	54.2	20.8	33.3
Feature	μ	h_1	h_2	h_3	h_4	h_5	h_6	h_7	h_8	ψ	φ_1	φ_2	φ_3	φ_4	φ_5	φ_6	φ_7	φ_8
Mean PoT	32.9±13.4									36.1±11.4								

Table 4. Number of effective features for each gender-age pair and ROIs. The number in a cell is the number of features (out of a total of 18) that are effective in the tests involving corresponding gender-age pairs and ROIs. For example, in the first column of the first row, 7 means that, in the first row of Table 2, 7 out of the 18 p-values corresponding to (FO,FY) in ROI 1 are smaller than or equal to 0.05.

	FO vs FY	FO vs MO	FO vs MY	FY vs MO	FY vs MY	MO vs MY
ROI 1	7	2	6	7	3	2
ROI 2	15	2	7	15	3	6
ROI 3	12	7	6	14	8	2
ROI 4	5	6	0	8	5	1
Mean	9.75	4.25	4.75	11.0	4.75	2.75

Figure legends

Figure 1. Example trabecular CBCT cubes cropped from left condyles in our study. From left to right: Female Younger (FY), Female Older (FO), Male Younger (MY), and Male Older (MO).

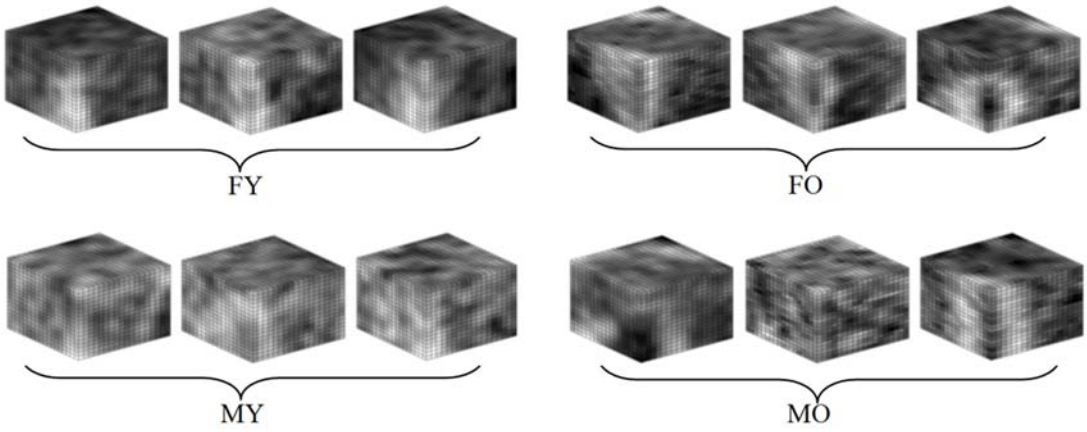

Fig. 2. P-values of all gender-age pairs over different ROIs and features.